Grid-connected Converters with Virtual Electromechanical Characteristics: Experimental Verification

Weiyi Zhang, *Student Member, IEEE*, Daniel Remon, *Student Member, IEEE*, Ignacio Candela, *Member, IEEE*, Alvaro Luna, *Member, IEEE*, and Pedro Rodriguez, *Fellow, IEEE*

***Abstract*—Grid-connected power converters, which are frequently used to link renewable generation plants with the grid, are required to provide a better functionality for large scale integration of renewables. They are expected to be grid-friendly, or even grid-supportive, instead of simply grid-feeding or grid-demanding. This paper designs a synchronous power controller for grid-connected converters in detail, emulating the electromechanical characteristics of synchronous machines and improving even its actual performance, as it is based on a virtual approach. Based on this design, the grid-interfacing units are capable of showing inertia, damping, and droop characteristics as synchronous machines and presenting thus a grid-supporting behavior. The detailed control design and experimental validation on a 10 kW laboratory setup acts as the main contribution of this paper, compared with the existing studies on generator emulation controls.**

***Index Terms*—DC-AC power conversion, power generation control, synchronous power controller, virtual electromechanical characteristics.**

I. Introduction

GENERATION plants based on renewable energy sources (RES) have increased their penetration into the electrical grid over the past years. The regulation capability of the grid can be reduced since the RES-based generation plants commonly follow the maximum power tracking laws, and do not interact with the grid.

Grid-connected converters commonly act as the interface between the RES-based generation plants and the grid [1], [2]. In many proposals, the steady-state performance of grid-connected converters has been specified b y d roop characteristics instead of through DC voltage balancing [3]–[7]. With the droop control, the active power generation is automatically adjusted by a primary frequency control, and the reactive power generation automatically supports the ac voltage. The converter can therefore interact with the grid with the aid of energy storage or curtailed power. In this manner, the regulation capability of the grid can be enhanced.

However, the dynamics of these converters still differ from those of the synchronous machine (SM), the total inertia in the grid does not increase along with the integration of RES-based generation plants. Therefore, the updated grid codes have taken the "synthetic inertia" into account [8], and intensive research activities on grid-connected converters with virtual electro-mechanical characteristics have been carried out since its first publication [9], including the sub-projects of China's 863 Plan in 2014. This trend is motivated by the fact that RES-based generation is increasing exponentially and grid-interactive loads with energy storage are also emerging.

Inertia emulation appears as the main objective in many works, and the implementation method can be categorized into the following types.

As the first type, the inertia emulation is realized using an extra loop in addition to the conventional control paradigm that comprises current control and power balancing (DC voltage control). Instead of using a DC voltage controller to balance the active power, the active power reference is specified according to a function of the grid frequency [10]–[12]. As an alternative, this extra loop method can also be used to specify the DC voltage reference following another function [13]. The main feature of this method is the minor changes to the conventional control structure. On the other hand, the derivative operation in the control structure and the dependence on the phase-locked loop (PLL) are the potential controversial points.

As the second type, the inertia emulation is realized in a modified PLL, which is proposed in [14]. Similar to the first type, this method entails only minor changes to the conventional control structure (only the change of the PLL).

The inertia emulation in the abovementioned two methods is both dependent on an external voltage source, and hence needs control scheme switching in order to form the grid in an island operation. In addition, even though the interaction dynamics between the converter and the grid is changed to emulate synchronous machines, the active power transfer dynamics is not yet the same as the one for synchronous machines.

Considering these two facts, the third type of method for

This work was partially supported by the Spanish Ministry of Economy and Competitiveness under the project ENE2014-60228-R.

W. Zhang (corresponding author, e-mail: weiyi.zhang@estudiant.upc.edu), D. Remon, I. Candela, and A. Luna are with Electrical Engineering Department, Technical University of Catalonia, Barcelona 08222, Spain.

P. Rodriguez is with Department of Engineering, University Loyola Andalucía, Seville 41014, Spain, and is also with Electrical Engineering Department, Technical University of Catalonia, Barcelona 08222, Spain.

inertia emulation emerged, which uses the power loop to specify inertia characteristics [15]–[26]. In this manner the active power transfer dynamics and power-frequency interaction dynamics are both changed, and the grid forming capability is achieved because of the existence of the converter output voltage reference, which is generated using the output of the active and reactive power loop. In this method, the grid synchronization is achieved by the power angle synchronization mechanism, other than the PLL that synchronizes the voltage phase.

As an alternative to the third type of method, the inertia emulation can also be realized by a DC voltage controller [27], [28].

Following the work of [18] referenced as Synchronous Power Controller (SPC), this paper conducts a detailed controller design based on the aforementioned concept. The grid-connected converters are enabled with inertia, damping, and droop characteristics, and hence possess a grid-supporting feature. Compared with the existing works, experimental validation and the associated analyses are particularly conducted, showing the feasibility of this proposal. The typical events such as changes in power orders and changes in grid frequency are considered, and the associated analyses include the realization of inertia, droop, and a comparison with the traditional vector current control.

The remaining part of this paper is organized as follows. In Section II, the control concept and implementation schemes of SPC are introduced. In Section III, the design of the power loop controller and the start-up techniques are presented. In Section IV, experimental results under different inputs are shown and analyzed. The conclusions are drawn in Section V.

II. Control Schemes

The overall control architecture is based on the SPC and external droop controllers. The SPC is an emulation and enhancement of the main electromechanical characteristics of synchronous machines, and droop control is used to provide ancillary services.

A. Synchronous Power Controller

The voltage source converter (VSC) controlled by the SPC is shown in Fig. 1. The controller structure comprises multiple blocks, such as the admittance block for emulating the electrical characteristics of synchronous machines and the power loop controller for emulating the mechanical characteristics.

SPC makes the VSC synchronized to the grid through power angle synchronization instead of voltage phase synchronization. The proposed system stems from the principle that a power converter can interact with the grid like a synchronous generator, by which the balance between the power generation and consumption is naturally kept through the speed variation of the rotor, thus achieving grid synchronization without needing any kind of PLL during normal operation. Considering the power converter case, this fact is an advantage as the power converter will be able to operate without being affected by any malfunction of the PLL. In some cases, an electrical system can experience a phase jump of more than 40º, which produces a transient in the PLL, and further undesired peculiar transients in the current control. By using the SPC, the control dynamics are not affected by the dynamics of the PLL. In addition, the inertial effect is not dependent on the connection to an external grid. So when the controlled VSC is disconnected from the main grids, it is able to maintain an island grid without any control scheme switching and keeps showing inertial characteristics.

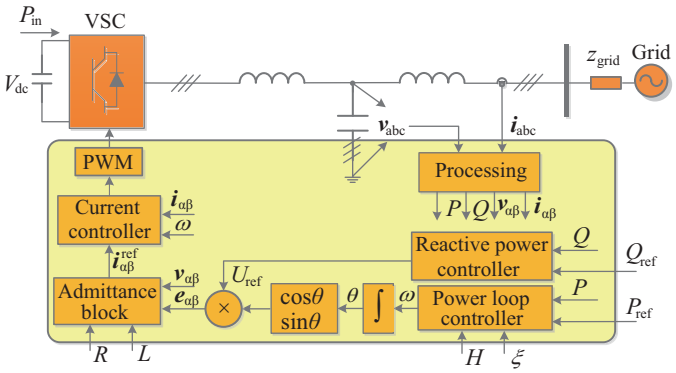

Fig. 1. The structure of the Synchronous Power Controller.

Regarding the design of the inner loops, an open-loop pulse width modulation (PWM) as in [16], [17], [29], or a voltage-current double-loop controller as in [24], [30] could be used. However, the open-loop PWM solution is unable to limit the current, and the double-loop solution poses issues in voltage source fighting. In addition, these strategies do not emulate the output impedance of synchronous machines, and thus do not naturally contribute to load sharing, and need impedance estimation when the VSC is connected to low X/R ratio networks. Since the impedance estimation becomes challenging when multiple generation units are connected in parallel, it is useful to emulate the output impedance of synchronous machines in the control design.

The virtual admittance used in this paper is shown in Fig. 2(a) [21], as an emulation of the synchronous machine stator. As shown in Fig. 2(a), the reactance and damping resistance are virtually implemented and can be adjusted.

The overall power transfer impedance will be dominated by the virtual admittance, which presents an X/R ratio much greater than 1, and the network impedance estimation is hence not needed. With the virtual admittance, the start-up transient can also be damped by using different admittance values in different operational stages. In this way, the controller structure and design become simple, since the back-up PLL as in [31] is not needed.

To configure the VSC to a current source, as shown in Fig. 2(a), a current controller is contained in the virtual admittance structure. It is able to control the current and further limit it with anti-windup measures, which is necessary in practice.

In several existing works, the output impedance of the synchronous machines is emulated by means of using a virtual impedance structure [4], and it has different implementation strategies. A generalization of the virtual impedance structure is shown in Fig. 2(b). In order to deal with the derivative

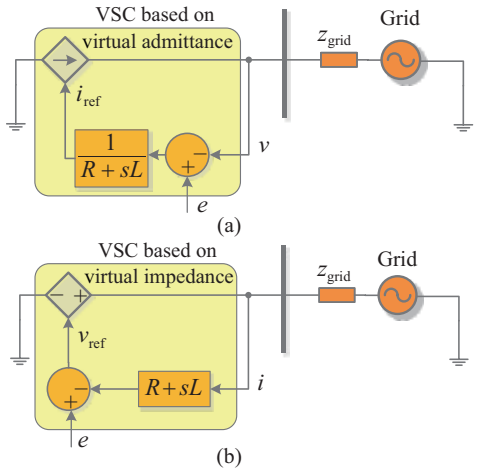

Fig. 2. Two strategies emulating the stator of the synchronous machines. (a) VSC based on virtual admittance (used in this paper). (b) VSC based on virtual impedance.

term contained in the structure, a low-pass filter is normally added to process the current measurement, or a fundamental frequency inductor ($j\omega_s L$) is used as a compromise. With a low-pass filter, the accurate emulation of the impedance cannot be achieved due to the phase shifts and delays. Moreover, the fundamental frequency inductor is not effective in the whole frequency range and it is not able to deal with load sharing [21]. By avoiding the derivative term, the virtual admittance structure shown in Fig. 2(a) does incur challenges in practical implementation. The voltage source fighting is avoided since the converter output voltage is not directly controlled. Moreover, only a current loop is needed in the virtual admittance structure, while for the virtual impedance implementation, a voltage-current cascaded double loop is necessary.

B. External Droop Controllers

Droop control is a typical control that a generation unit should provide to the grid, and it is also needed in forming an independent grid. The virtual admittance determines the inherent Q-V droop characteristics, and the power loop controller of the SPC can determine the inherent P-f droop characteristics. Nevertheless, external P-f and Q-V droop controllers are also needed to modify the inherent droop characteristics and define the overall droop slope. The schemes of the external droop controllers are shown in Fig. 3.

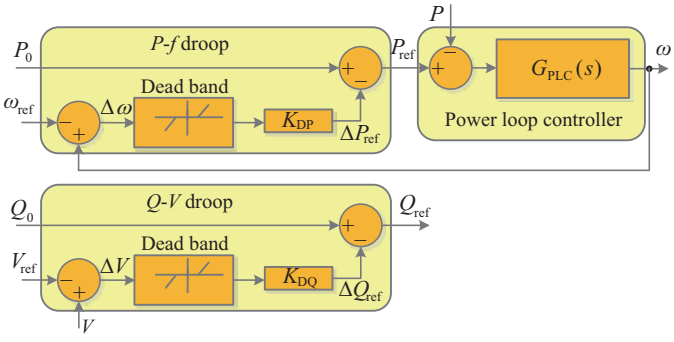

Fig. 3. The schemes of the external droop controllers.

Based on the synchronization mechanism of the SPC, the input frequency measurement is provided by the output of the power loop controller. In the layout, K_{DP} and K_{DQ} are the droop slope for each controller. Commonly in practice, a dead band is used in the droop loop to disable the droop controller around the nominal frequency.

III. Power Loop Synchronization and Inertia Emulation

The power angle synchronization is not achieved by a single loop like PLL, instead, the power loop controller, virtual admittance and current controller altogether achieve the power angle synchronization.

The mathematical model of the power control loop is shown in Fig. 4. It is a generalized modeling of the active power control mechanisms achieved by the control structure of Fig. 1.

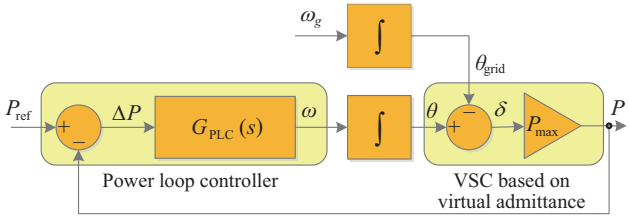

Fig. 4. Mathematical model of the SPC power control.

The relationship between the active power generation P and the voltage angle difference δ is written as,

$$P = P_{\max}\delta \tag{1}$$

where δ is the voltage-angle difference between the inner voltage e and the grid voltage v. The transfer gain is shown as,

$$P_{\max} = \frac{EV}{X} \tag{2}$$

where E and V are the rms of the inner voltage, e, and the grid voltage, v, respectively, and X is the virtual output reactance, which is defined by the admittance block in the case when SPC is used. During the modeling and analysis, V can be given the nominal value, and E can be estimated approximately equal to V, while X will be specified by setting the value of L of the virtual admittance.

The VSC based on virtual admittance can be modeled as shown in Fig. 4 because of two facts: 1) The power is delivered based on the load angle and reactance (that predominates the whole impedance) as shown in (1); and 2) The inner current controller is significantly faster than the power loop controller with inertial effect, hence its dynamics can be decoupled from the modeling of the power control loop to reduce its complexity.

Unlike the conventional converter control strategies that require a dedicated synchronization block and a dedicated power controller, the designed power control loop is able to achieve synchronization as well as controlling the active power, as occurs naturally in a synchronous machine. In this way, it is possible to give inertia characteristics by configuring the power loop controller, while a PLL is not used.

The synchronous angular speed ω is adjusted according to the error in power regulation, and will further move the load angle to regulate the power. Then ω can be regulated to diminish the power control error, and meanwhile maintain the synchronization with the grid frequency ω_{g}.

A. Implementation of SM Swing Equation

To replicate the swing equation of the synchronous machines, (3) can be selected as the power loop controller [32].

$$G_{\mathrm{PLC}}(s) = \frac{\omega_{\mathrm{s}}}{2HS_{\mathrm{N}}s + \omega_{\mathrm{s}}^2 D} \tag{3}$$

where ω_{s} is the grid rated angular speed, H and D the inertia and damping constant, respectively, and S_{N} the rated power of the converter. It is known that the damping characteristics of the synchronous machines are mechanically and electrically constrained. However, as shown in (3), once the swing equation is virtually implemented, the damping performance can be improved by tuning D.

Using the form shown in (3) as the power loop controller, the transfer function of the active power control loop is written as,

$$\frac{\partial P}{\partial P_{\mathrm{ref}}}(s) = \frac{\omega_{\mathrm{n}}^2}{s^2 + 2\xi\omega_{\mathrm{n}}s + \omega_{\mathrm{n}}^2}, \tag{4a}$$

$$\xi = \frac{D\omega_{\mathrm{s}}}{2}\sqrt{\frac{\omega_{\mathrm{s}}}{2HS_{\mathrm{N}}P_{\max}}}, \tag{4b}$$

$$\omega_{\mathrm{n}} = \sqrt{\frac{P_{\max}\omega_{\mathrm{s}}}{2HS_{\mathrm{N}}}}. \tag{4c}$$

Obviously the dynamics defined by (4a) is dependent on the parameters ω_{n} and ξ. Further, ω_{n} and ξ are dependent on the inertia and damping parameters H and D as shown in (4b) and (4c). It is worth noting that the damping coefficient ξ should be fixed to a value greater than zero to ensure the local stability.

In addition to the transient response to power reference changes (4a), the performance, based on the presence of frequency changes, should also be analyzed as another aspect of the power loop dynamics. The transfer function is written as,

$$\frac{\partial P}{\partial \omega_{\mathrm{g}}}(s) = \frac{-P_{\max}(s + 2\xi\omega_{\mathrm{n}})}{s^2 + 2\xi\omega_{\mathrm{n}}s + \omega_{\mathrm{n}}^2}. \tag{5}$$

A steady-state power-frequency droop slope D_{P} can be determined by (5), and (6) is obtained.

$$D_{\mathrm{P}} = \left|\frac{\partial P}{\partial \omega_{\mathrm{g}}}(0)\right| = \frac{2\xi P_{\max}}{\omega_{\mathrm{n}}} \tag{6}$$

Let $1/R_{\mathrm{D}}$ denote the per unit value of the power-frequency droop slope, (which is typically 5% in the case of a traditional generation unit [33]), R_{D} can be expressed in terms of D_{P} as shown in (7).

$$R_{\mathrm{D}} = \frac{D_{\mathrm{P}}\omega_{\mathrm{s}}}{S_{\mathrm{N}}} \tag{7}$$

Substituting the D_{P} in (7) using (6) and further substituting ω_{n} using (4c), the relationship among the damping, inertia and droop slope is shown as,

$$\frac{1}{R_{\mathrm{D}}} = \frac{1}{2\xi}\sqrt{\frac{S_{\mathrm{N}}}{2HP_{\max}\omega_{\mathrm{s}}}}. \tag{8}$$

The per-unit virtual reactance X_{pu} is written as,

$$X_{\mathrm{pu}} = \frac{X}{EV/S_{\mathrm{N}}} = \frac{S_{\mathrm{N}}}{P_{\max}}, \tag{9}$$

and then (8) evolves to (10) in terms of X_{pu}.

$$\frac{1}{R_{\mathrm{D}}} = \frac{1}{2\xi}\sqrt{\frac{X_{\mathrm{pu}}}{2H\omega_{\mathrm{s}}}} \tag{10}$$

Fig. 5 shows the constraint between the inertia and damping parameters, which is plotted using (10). Four cases are considered, and the inertia constant H is fixed to different values in each case, while X_{pu} is fixed to 0.3.

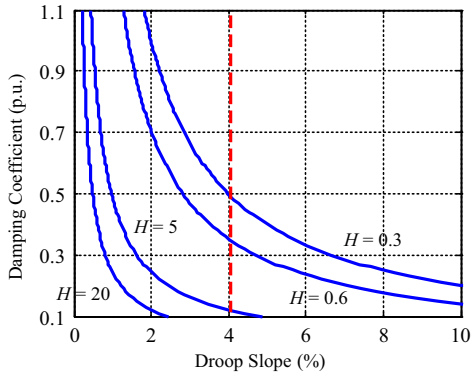

Fig. 5. The constraint between the damping characteristics and the P-f droop characteristics.

When $1/R_{\mathrm{D}}$ is specified to 4%, as shown in Fig. 5, ξ will be smaller than 0.5, which is smaller than the optimal damping coefficient for a second-order transfer function (0.7). If a greater value of $1/R_{\mathrm{D}}$ is requested by the transmission system operator, ξ needs to be reduced further.

The denominator of the right part of (10) will not be zero under proper inertia and damping parameters, and then $1/R_{\mathrm{D}}$ cannot be infinite. Therefore, the droop characteristics cannot be totally eliminated by tuning parameters. Then an external droop controller is needed to compensate the intrinsic droop for a fixed power control, or to modify the internal droop slope for the desired droop slope.

B. PI-based Power Loop Controller

When the power loop controller is designed as (3) for the replication of the SM swing equation, an additional droop controller is necessary in both the fixed power control mode and droop mode operation. As an alternative to the controller form (3), the PI controller shown in (11) is proposed as the power loop controller.

$$G_{\mathrm{PLC}}(s) = K_{\mathrm{X}} + \frac{K_{\mathrm{H}}}{s} \tag{11}$$

The PI-based power loop controller leads to a zero steady-state error of active power control even in the presence of grid frequency changes. In this way, the fixed power control mode can be simply achieved by disabling the external droop loop. And for the droop control mode, the parameter setting of the external droop controller will be straightforward and simple.

In addition, the inertia and damping characteristics can also be given by assigning proper values to the control parameters.

Using the form shown in (11) as the power loop controller, the transfer function of the active power control loop is written as (12a), which is also a second-order transfer function like (4a), and the dynamics can easily be analyzed. The parameters ξ and ω_{n} are defined in (12b) and (12c).

$$\frac{\partial P}{\partial P_{\mathrm{ref}}}(s) = \frac{2\xi\omega_{\mathrm{n}}s + \omega_{\mathrm{n}}^2}{s^2 + 2\xi\omega_{\mathrm{n}}s + \omega_{\mathrm{n}}^2} \tag{12a}$$

$$\xi = \frac{P_{\max}K_{\mathrm{X}}}{2\omega_{\mathrm{n}}} \tag{12b}$$

$$\omega_{\mathrm{n}} = \sqrt{P_{\max}K_{\mathrm{H}}} \tag{12c}$$

The numerator of (12a) is different from (4a), while the denominator is the same. Hence, the condition for local stability is not changed. The inertia and damping characteristics can be defined by fixing the control parameters K_{X} and K_{H} following the relationship of (12b) and (12c).

The active power response under grid frequency changes is analytically written as,

$$\frac{\partial P}{\partial \omega_{\mathrm{g}}}(s) = \frac{-P_{\max}s}{s^2 + 2\xi\omega_{\mathrm{n}}s + \omega_{\mathrm{n}}^2}, \tag{13}$$

and the steady-state droop slope is calculated as,

$$D_{\mathrm{P}} = \left|\frac{\partial P}{\partial \omega_{\mathrm{g}}}(0)\right| = 0. \tag{14}$$

This equation indicates that the generated power will always track the power reference in the steady state regardless of the frequency variations. Hence, when the converter is required to operate in the fixed power control mode, an additional droop control is not needed. In case the droop mode operation is needed, the droop slope can be directly set by the external droop controller.

C. Setting of Control Parameters

According to (12b) and (12c), the control parameters K_{X} and K_{H} can be calculated based on the specifications of ξ and ω_{n}. In addition, the natural frequency ω_{n} can be translated to the inertia constant H by combining (4c) and (12c) to equate the ω_{n} from the two cases. The control parameters can be fixed in advance, or optionally, be adaptive following the inputs of H and ξ, thus a flexible control is available.

The value of H is equivalent to the inertia constant of the synchronous machines, and it needs to be specified taking into account the constraints of the power reserve. The damping coefficient ξ can be specified within the range $0 < \xi < 1$ to make the system stable and under damped.

For tuning the damping coefficient ξ, the transfer function (12a) is imposed by a step input, and the settling time and overshoot of the transient response based on different values of ξ are analyzed. The relationship between the damping coefficient ξ and the step response overshoot is plotted in Fig. 6.

As an example shown in Fig. 6, the step response overshoot will be below 20% once the damping coefficient is fixed greater than 0.73. Fig. 6 shows that different values of H do not lead to a significant difference in the damping characteristics, and the curves under two different values of H almost coincide with each other.

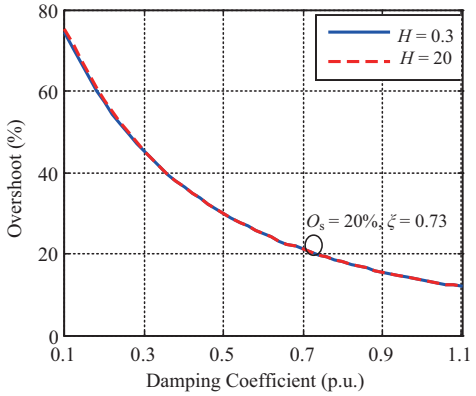

Fig. 6. The relationship between the damping coefficient ξ and the step response overshoot.

D. Start-up Based on Virtual Admittance Scheduling

The admittance block shown in Fig. 1 is expressed as,

$$\boldsymbol{i}_{\alpha\beta}^{\mathrm{ref}} = \frac{1}{R + sL}(\boldsymbol{e}_{\alpha\beta} - \boldsymbol{v}_{\alpha\beta}). \tag{15}$$

By scheduling the parameters of the admittance, namely R and L, a smooth start-up and grid connection can be achieved. Fig. 7 shows the simulated start-up process as an example.

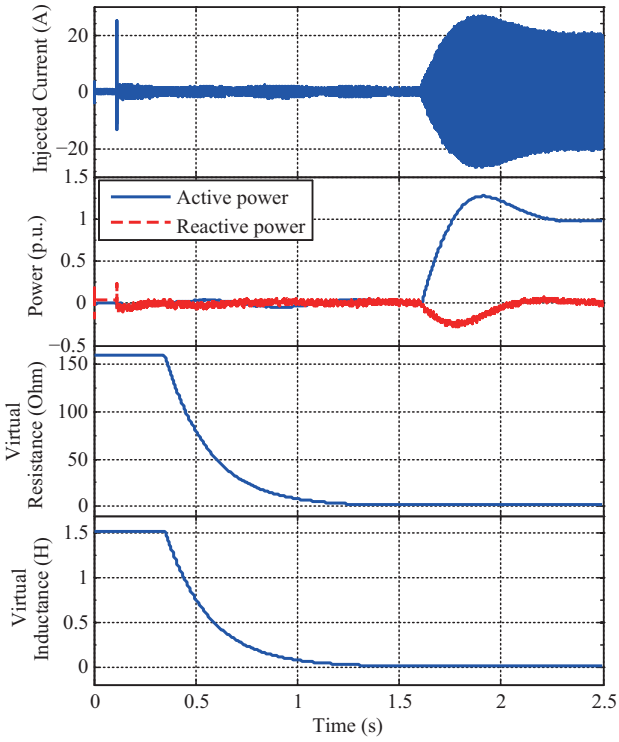

Fig. 7. Start-up process based on virtual admittance scheduling.

In order to limit the current transient at the moment of connection, the initial values for R and L are set significantly greater than the nominal ones. At 0.11 s, the switching of

the VSC is enabled, the injected current experiences a fast transient, and the current magnitude is within the acceptable range. At 0.35 s the synchronization is completed, and the values of R and L start to be reduced gradually to the nominal values during 1 s. At 1.6 s, after the nominal values of R and L are reached, the VSC can operate normally and increases the active power injection to the nominal.

A zoom-in of the start-up process at $0.05 \text{ s} < t < 0.35$ s is shown in Fig. 8, in which the details of the synchronization process are shown. It is seen that both the α and β components of the virtual electromotive force e can be gradually shifted to be synchronized with the grid voltage v in several grid cycles.

It is worth mentioning that the parameters transition time can be predefined in the embedded converter controller or given by secondary orders.

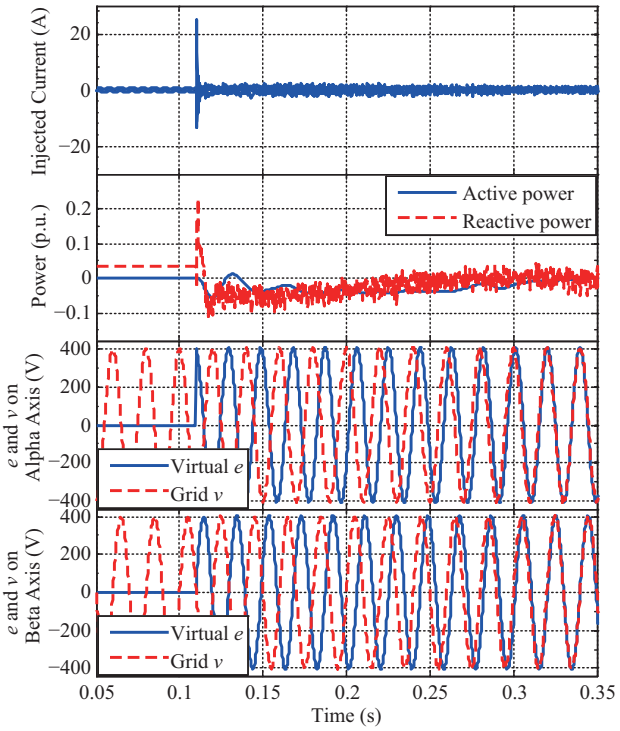

Fig. 8. Grid synchronization process of the VSC.

IV. Experimental Results

In the experimental validation, a 10 kW grid-connected converter test platform is used for implementing the proposed controller. Fig. 9(a) shows the test platform scheme, and Fig. 9(b) shows the laboratory setups.

The power rating of the DC power source is 40 kW, and it is connected to the DC bus. Using a DC voltage source, the DC bus voltage can be fixed for providing sufficient power reserve. A regenerative AC source forms the AC grid, in this way the voltage magnitude and frequency can be specified and adjusted. The controller is coded in a dSPACE 1103 system. The key parameters of the setups and the controller are shown in Table I. The SPC based on the PI-based power loop controller is implemented, and the results from 5 sets of tests are shown.

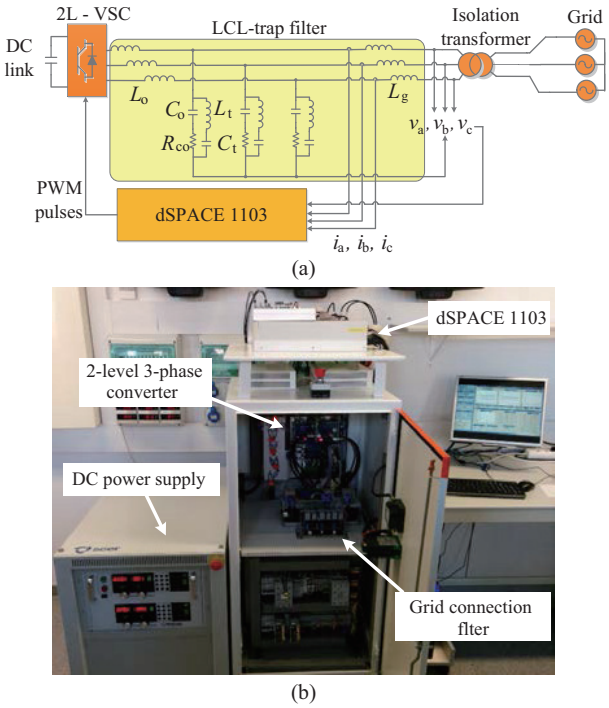

Fig. 9. 10 kW experimental test platform. (a) Test platform scheme, (b) Laboratory environment.

TABLE I
Key Experimental Tests Parameters

Symbol	Definition	Value
V_{DC}	DC-link voltage (V)	640
V_g	Grid phase-to-phase voltage RMS (V)	400
f_g	Grid nominal frequency (Hz)	50
S_N	Nominal power (kW)	10
f_{sw}	Switching frequency (Hz)	10,050
ξ	Damping coefficient (p.u.)	0.73
R_{pu}	Virtual resistance (p.u.)	0.1
X_{pu}	Virtual reactance (p.u.)	0.3

First, a step change in the power reference from 0.5 p.u. to 1 p.u. is given to validate the dynamic performance. To clearly show the inertia characteristics, H is designated to be 10 s as a great value. The grid voltage and injected current waveforms are shown in Fig. 10, and the active power, reactive power, virtual synchronous frequency ω and the phase of the electromotive force θ are plotted in Fig. 11.

As shown in the results, the grid injected current and power change in a ramp, showing the typical response of a second-order system. The transient response without any oscillations also indicates a proper damping of the system. And in the steady state, the injected active and reactive power is accurately controlled.

The active power profile is compared with the predicted trajectory as shown in Fig. 11, and the power response complies with the defined inertia characteristics. The predicted trajectory is calculated by imposing a step input in the transfer function shown in (12a). The virtual synchronous frequency ω is also shown in the figure, and the grid synchronization is achieved. The phase signal θ is used to generate the virtual electromotive force, and in the controller coding, it needs to

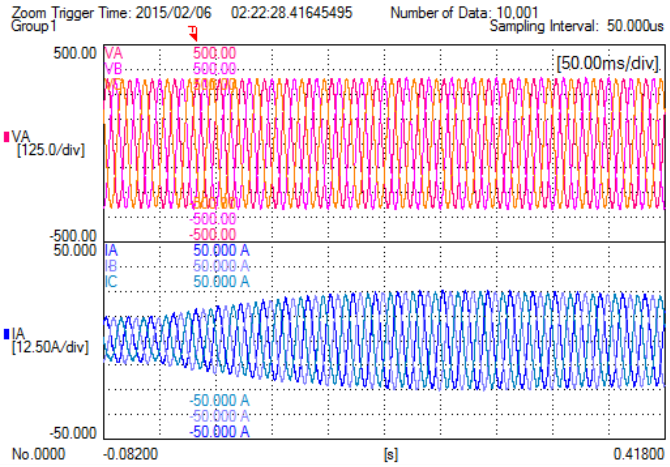

Fig. 10. Grid voltage and injected current in the presence of a power reference step.

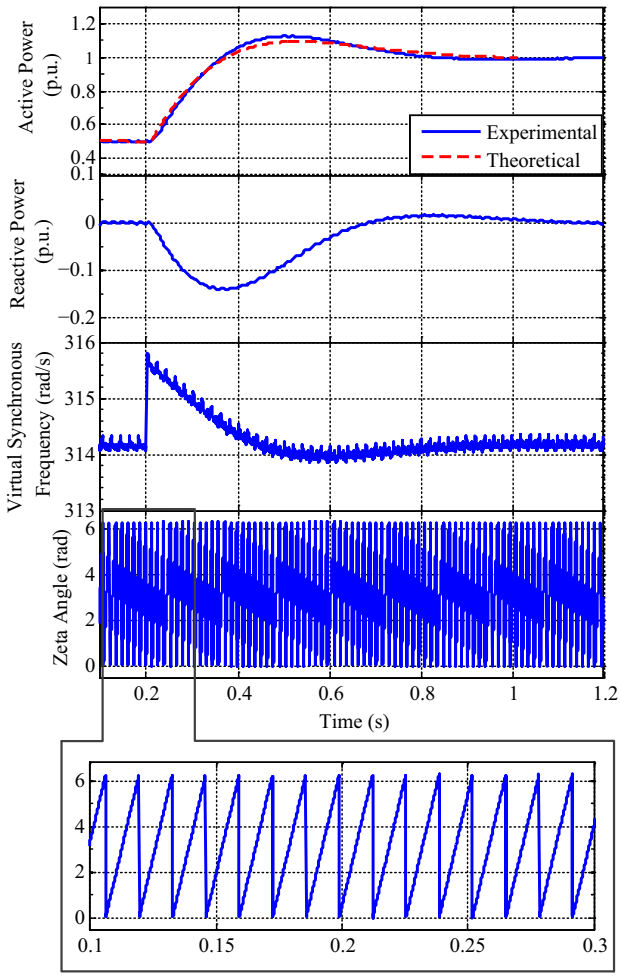

Fig. 11. Responses in the presence of the power reference step.

be constrained in a limited range to avoid a variable overflow. As shown in Fig. 11, θ is always subtracted by 2π once it is over 2π.

Secondly, variations of the grid frequency are imposed by configuring the AC regenerative power source, and the frequency changing slope is made to $\pm$ 1 Hz/s. The response of the injected current, active and reactive power and virtual synchronous frequency are respectively shown in Fig. 12. The active power reference is set to 0.5 p.u. and the reactive power reference to 0, and the inertia constant is kept the same as in the previous test. The gain of the external droop controller K_{DP} is set to 0.

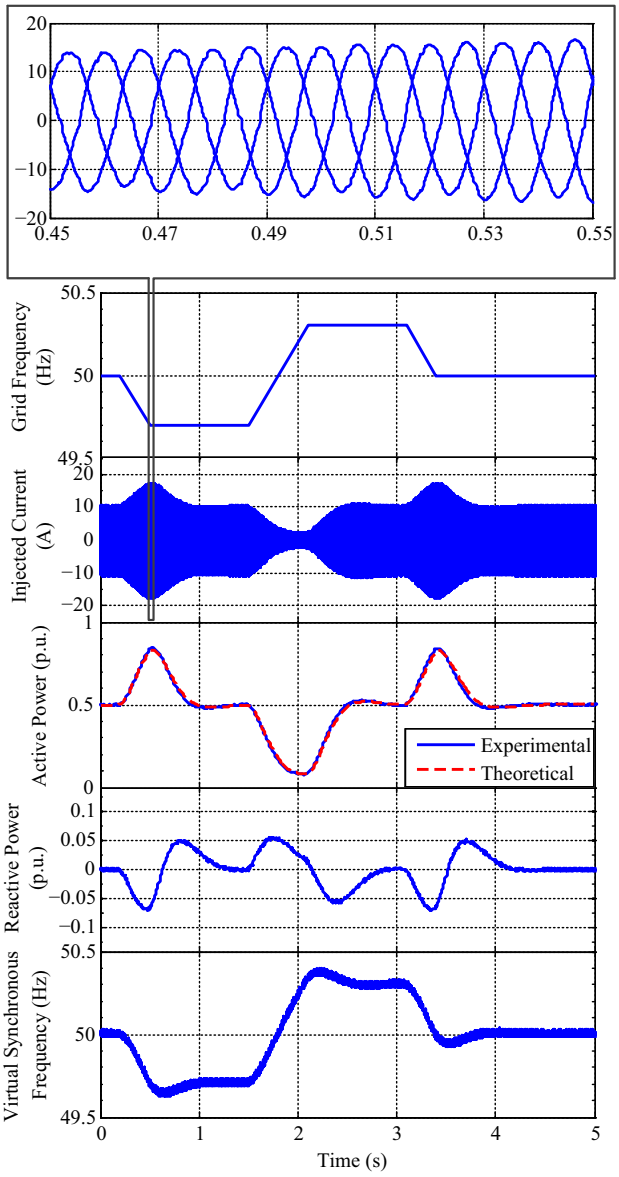

Fig. 12. Responses in the presence of the grid frequency disturbances.

According to the results, the injected current and power counteract the deviation of the grid frequency, showing a grid-supporting behavior. The controlled active and reactive power goes back to its reference in a steady state, presenting the accurate control of active and reactive power.

Particularly, the predicted trajectory of active power is calculated by imposing the same grid frequency variations in the transfer function shown in (13), and compared with the actual active power profile in Fig. 12. It validates the accurate implementation of the designed inertia characteristics. The perfect match between the predicted and actual power response also relies on the fact that the reference of the inner current

loop does not experience drastic changes due to the inertia of the power loop, thus the current loop dynamics is not coupled in the response. In addition, the virtual synchronous frequency ω shows an accurate lock of the grid frequency in the steady state as well as the inertia dynamics.

Thirdly, the inertia characteristics are further validated in Fig. 13. Power step responses under different H are shown.

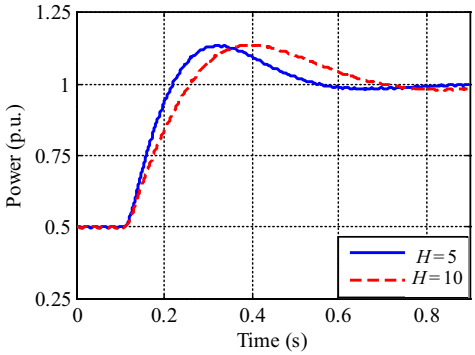

Fig. 13. Responses to the power reference step changes under different inertia constants.

It is demonstrated that the time response can be adjusted through specifying the inertia constant H. Since the natural frequency ω_{n} is inversely proportional to the square root of the inertia constant H, the time of response is approximately proportional to the square root of H. This fact is validated by Fig. 13, where the settling time of the two responses are calculated respectively to be 479.0 ms and 677.5 ms. The settling time when $H = 10$ is close to the settling time when $H = 5$ multiplied by $\sqrt{2}$.

Fourthly, the performance of the external droop controller is validated. The droop slope is specified to be 2% by designating K_{DP} to 1591.5 W/(rad/s). And the dead band ω_{db} is set to 0 for simplicity. In the test, the active power reference of the converter is set to 0, and the grid frequency is reduced step by step from the nominal value. At each value of frequency, the steady-state power is obtained from the data recorded by the power analyzer. The steady-state power-frequency relationship is plotted in Fig. 14, where the slope of the data outline corresponds to the designation.

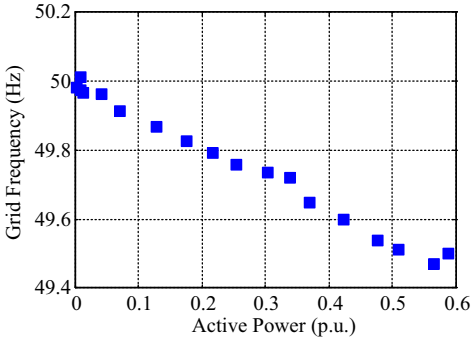

Fig. 14. Power-frequency droop characteristics under a 2% droop slope.

At last, the performance of the SPC is compared with a typical PLL-based vector current control (VCC) strategy. Both strategies are accompanied by external droop controllers and specified with the same droop slope, namely 2%, and the same dead band, namely 0.05 Hz. The responses under grid frequency variations are compared in Fig. 15.

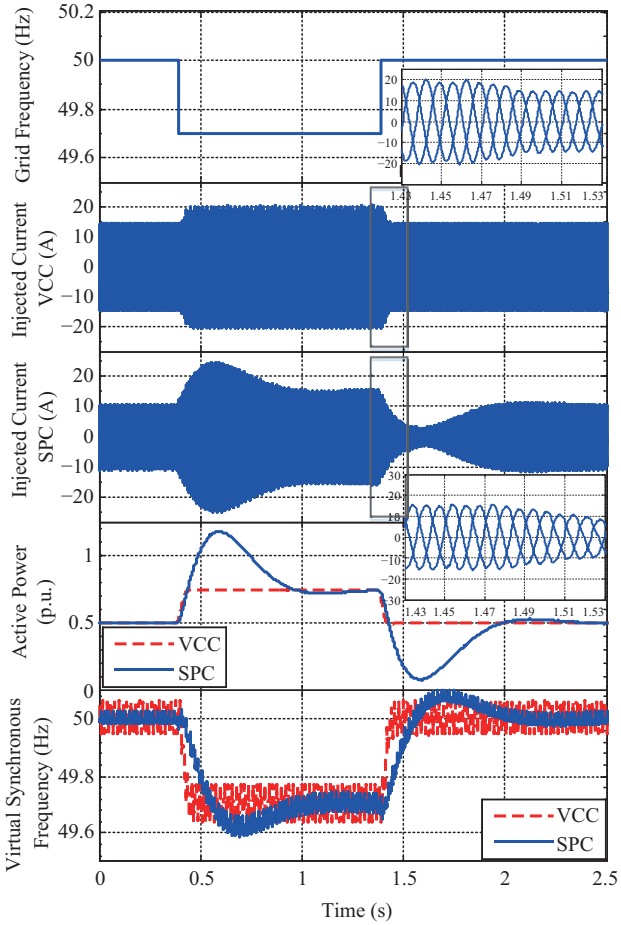

Fig. 15. SPC compared with PLL-based vector current control in the presence of frequency disturbances.

In order to highlight the differences of these two strategies in the grid-interactive dynamics, the grid frequency is configured to change in steps, which does not normally occur in realistic systems. The responses of the current, active power and synchronous frequencies that are controlled by SPC and VCC are respectively shown in Fig. 15. Comparing these two figures, the SPC-controlled converter shows a stronger effect in transient to counteract the frequency deviation because of the inertia characteristics. When the grid frequency drops, the grid angle decreases, so the SPC-controlled converter injects more power. The power imbalance modifies the virtual frequency and θ until a new equilibrium is reached. In this transient the converter frees part of its virtual kinetic energy, naturally compensating the frequency drop. Therefore, with enough installations, SPC-controlled converters will considerably contribute to the frequency stabilization.

V. Conclusion

This paper designed the Synchronous Power Controller in detail for realizing grid-connected converters with virtual

electromechanical characteristics. Features like inertia and damping are incorporated in the power loop controller, and the grid frequency stabilization is hence enhanced. The grid synchronization can be achieved by the power angle synchronization such as the mechanisms of synchronous machines, while the commonly used PLL can be eliminated. Therefore, the converters are able to be connected to weak grids that have limited short circuit capacity. In addition, the virtual admittance can contribute in delivering power to low X/R ratio grids, which is the case of many low-voltage grids. And the admittance value can be adjusted online for different operational stages.

Experimental results were conducted on a laboratory-scale grid-connected converter, providing a preliminary validation of the SPC concept. Both in the presence of power order changes and grid frequency disturbances, the active power responses clearly follow the specified inertia characteristics. By comparing the SPC and the typical VCC, the converter controlled by the SPC shows a stronger power response in transient to oppose grid frequency disturbances. The effectiveness of the external droop controller is verified as well.

ACKNOWLEDGMENT

This work has been partially supported by the Spanish Ministry of Economy and Competitiveness under the project ENE2014-60228-R. W. Zhang expresses gratitude to the China Scholarship Council for supporting his Ph. D. study in the specified time framework. Any opinions, findings and conclusions or recommendations expressed in this material are those of the authors and do not necessarily reflect those of the host institutions or funders.

REFERENCES

[1] L. J. Chen and S. W. Mei, "An integrated control and protection system for photovoltaic microgrids," *CSEE Journal of Power and Energy Systems*, vol. 1, no. 1, pp. 36–42, Mar. 2015.

[2] G. F. Tang, Z. Y. He, H. Pang, X. M. Huang, and X.-P. Zhang, "Basic topology and dey devices of the five-ternimal DC grid," *CSEE Journal of Power and Energy Systems*, vol. 1, no. 2, pp. 22–35, Jun. 2015.

[3] A. Engler and N. Soultanis, "Droop control in LV-grids," in *International Conference on Future Power Systems*, 18 Nov. 2005, pp. 1–6.

[4] J. M. Guerrero, J. C. Vasquez, J. Matas, L. G. de Vicuña, and M. Castilla, "Hierarchical control of droop-controlled AC and DC microgrids – A general approach toward standardization," *IEEE Transactions on Industrial Electronics*, vol. 58, no. 1, pp. 158–172, Jan. 2011.

[5] T. Loix, K. de Brabandere, J. Driesen, and R. Belmans, "A three-phase voltage and frequency droop control scheme for parallel inverters," in *Proceedings of IECON 2007 – 33rd Annual Conference of the IEEE Industrial Electronics Society*, 5–8 Nov. 2007, pp. 1662–1667.

[6] J. Rocabert, A. Luna, F. Blaabjerg, and P. Rodríguez, "Control of power converters in AC microgrids," *IEEE Transactions on Power Electronics*, vol. 27, no. 11, pp. 4734–4749, Nov. 2012.

[7] K. de Brabandere, B. Bolsens, J. V. D. Keybus, A. Woyte, J. Driesen, and R. Belmans, "A voltage and frequency droop control method for parallel inverters," *IEEE Transactions on Power Electronics*, vol. 22, no. 4, pp. 1107–1115, Jul. 2007.

[8] Entso-E. (2012, Jun.). ENTSO-E network code for requirements for grid connection applicable to all generators. [Online]. Available: https://www.entsoe.eu/fileadmin/user_upload/_library/consultations/Network_Code_RfG/120626_final_Network_Code_on_Requirements_for_Grid_Connection_applicable_to_all_Generators.pdf

[9] H. P. Beck and R. Hesse, "Virtual synchronous machine," in *Proceedings of 9th International Conference on Electrical Power Quality and Utilisastion, EPQU 2007*, 9–11 Oct. 2007, pp. 1–6.

[10] T. K. Vrana and C. Hille, "A novel control method for dispersed converters providing dynamic frequency response," *Electrical Engineering*, vol. 93, no. 4, pp. 217–226, Dec. 2011.

[11] M. A. Torres, L. A. C. Lopes, L. A. Morán, and J. R. Espinoza, "Self-tuning virtual synchronous machine: A control strategy for energy storage systems to support dynamic frequency control," *IEEE Transactions on Energy Conversion*, vol. 29, no. 4, pp. 833–840, Dec. 2014.

[12] S. I. Nanou, A. G. Papakonstantinou, and S. A. Papathanassiou, "A generic model of two-stage grid-connected PV systems with primary frequency response and inertia emulation," *Electric Power Systems Research*, vol. 127, pp. 186–196, Oct. 2015.

[13] J. B. Zhu, C. D. Booth, G. P. Adam, A. J. Roscoe, and C. G. Bright, "Inertia emulation control strategy for VSC-HVDC transmission systems," *IEEE Transactions on Power Systems*, vol. 28, no. 2, pp. 1277–1287, May 2013.

[14] M. P. N. van Wesenbeeck, S. W. H. de Haan, P. Varela, and K. Visscher, "Grid tied converter with virtual kinetic storage," in *2009 IEEE Bucharest PowerTech*, 28 Jun.–2 Jul. 2009, pp. 1–7.

[15] F. Gao and M. R. Iravani, "A control strategy for a distributed generation unit in grid-connected and autonomous modes of operation," *IEEE Transactions on Power Delivery*, vol. 23, no. 2, pp. 850–859, Apr. 2008.

[16] Q. C. Zhong and G. Weiss, "Synchronverters: Inverters that mimic synchronous generators," *IEEE Transactions on Industrial Electronics*, vol. 58, no. 4, pp. 1259–1267, Apr. 2011.

[17] S. M. Ashabani and Y. A. R. I. Mohamed, "A flexible control strategy for grid-connected and islanded microgrids with enhanced stability using nonlinear microgrid stabilizer," *IEEE Transactions on Smart Grid*, vol. 3, no. 3, pp. 1291–1301, Sep. 2012.

[18] P. Rodriguez, J. I. Candela, J. Rocabert, and R. Teodorescu, "Synchronous power controller for a generating system based on static power converters," International Patent WO 2012/117 131 A1, Sep. 7, 2012,

[19] P. Rodriguez, I. Candela, and A. Luna, "Control of PV generation systems using the synchronous power controller," in *Proceedings of 2013 IEEE Energy Conversion Congress and Exposition (ECCE)*, 2013, pp. 993–998.

[20] Y. Hirase, K. Abe, K. Sugimoto, and Y. Shindo, "A grid-connected inverter with virtual synchronous generator model of algebraic type," *Electrical Engineering in Japan*, vol. 184, no. 4, pp. 10–21, Sep. 2013.

[21] P. Rodriguez, I. Candela, C. Citro, J. Rocabert, and A. Luna, "Control of grid-connected power converters based on a virtual admittance control loop," in *2013 15th European Conference on Power Electronic and Applications (EPE)*, 2–6 Sep. 2013, pp. 1–10.

[22] S. D'Arco and J. A. Suul, "Equivalence of virtual synchronous machines and frequency-droops for converter-based microgrids," *IEEE Transactions on Smart Grid*, vol. 5, no. 1, pp. 394–395, Jan. 2014.

[23] J. Alipoor, Y. Miura, and T. Ise, "Power system stabilization using virtual synchronous generator with alternating moment of inertia," *IEEE Journal of Emerging Selected Topics in Power Electronics*, vol. 3, no. 2, pp. 451–458, Jun. 2015.

[24] M. Y. Guan, W. L. Pan, J. Zhang, Q. R. Hao, J. Z. Cheng, and X. Zheng, "Synchronous generator emulation control strategy for voltage source converter (VSC) stations," *IEEE Transactions on Power Systems*, vol. 30, no. 6, pp. 3093–3101, Nov. 2015.

[25] S. Wang, J. B. Hu, and X. M. Yuan, "Virtual synchronous control for grid-connected DFIG-based wind turbines," *IEEE Journal of Emerging Selected Topics in Power Electronics*, vol. 3, no. 4, pp. 932–944, Dec. 2015.

[26] M. Ashabani, F. D. Freijedo, S. Golestan, and J. M. Guerrero, "Inducverters: PLL-less converters with auto-synchronization and emulated inertia capability," *IEEE Transactions on Smart Grid*, vol. 7, no. 3, pp. 1660–1674, May 2016.

[27] D. Remon, A. M. Cantarellas, E. Rakhshani, I. Candela, and P. Rodriguez, "An active power synchronization control loop for grid-connected converters," in *2014 IEEE PES General Meeting, Conference & Exposition*, 27–31 Jul. 2014, pp. 1–5.

[28] H. Alatrash, A. Mensah, E. Mark, G. Haddad, and J. Enslin, "Generator emulation controls for photovoltaic inverters," *IEEE Transactions on Smart Grid*, vol. 3, no. 2, pp. 996–1011, Jun. 2012.

[29] K. Sakimoto, Y. Miura, and T. Ise, "Stabilization of a power system with a distributed generator by a virtual synchronous generator function," in *2011 IEEE 8th International Conference on Power Electronics and ECCE Asia (ICPE & ECCE)*, 30 May–3 Jun. 2011, pp. 1498–1505.

[30] S. D'Arco, J. A. Suul, and O. B. Fosso, "Control system tuning and stability analysis of virtual synchronous machines," in *2013 IEEE Energy Conversion Congress and Exposition (ECCE)*, 15–19 Sep. 2013, pp. 2664–2671.

[31] L. D. Zhang, L. Harnefors, and H. P. Nee, "Power-synchronization control of grid-connected voltage-source converters," *IEEE Transactions on Power Systems*, vol. 25, no. 2, pp. 809–820, May 2010.
[32] P. Kundur, *Power System Stability and Control*. New York, USA: McGraw-Hill, 1994.
[33] J. Duncan Glover, M. S. Sarma, and T. J. Overbye, *Power System Analysis and Design*, 4th ed. USA: Cengage Learning, 2010.

Weiyi Zhang (S'15) received a B.Eng. in Electrical Engineering and M.Sc. in Power Electronics and Electrical Drive from the Northwestern Polytechnical University, Xi'an, China, in 2010 and 2013, respectively. He has been working toward a Ph.D. degree at the research center on Renewable Electrical Energy Systems (SEER) in the Technical University of Catalonia, Spain since 2013. His current research interests include control of power converters and integration of distributed generation systems.

Daniel Remon (S'15) received a degree in Electrical Engineering, and a degree in Mathematics, from the Technical University of Catalonia (UPC), Barcelona, Spain, in 2012, and a M.Sc. degree in Electrical Energy Systems from the University of Seville, Seville, Spain, in 2015. He is currently working toward a Ph.D. degree in Electrical Energy Systems at the UPC, and has been a visiting student at the University of Waterloo, Ontario, Canada, from 2015 to 2016, with the support of a "la Caixa" grant.

He was with Abengoa, Seville, Spain, as an industrial PhD fellow from 2013 to 2015. His current research interests include renewable energy integration in transmission and distribution systems, power system modeling, stability and control, and electricity markets.

Ignacio Candela (M'04) received B.S. and M.S. degrees in Industrial Engineering in 1987 and 2000, respectively, and his Ph.D. degree in Electrical Engineering in 2009, all from the Technical University of Catalonia (UPC), Barcelona, Spain. In 1990, he became an Assistant Professor at UPC, where he later advanced to Associate Professor in 1993. Currently he is part of the research group on Renewable Electrical Energy Systems, Department of Electrical Engineering. He has authored or coauthored more than 80 published technical papers, and holds several patents. His current research interests include power conditioning, integration of distributed energy systems, and control of grid connected power converters. Dr. Candela is a member of the IEEE Power Electronics Society, the IEEE Industrial Electronics Society, and the IEEE Industry Application Society.

Alvaro Luna (M'10) received B.Sc., M.Sc., and Ph.D. degrees from the Technical University of Catalonia (UPC), Barcelona, Spain, in 2001, 2005, and 2009, respectively, all in electrical engineering. He joined as a Faculty Member at UPC in 2005, where he is currently an Assistant Professor. His research interests include wind turbines control, PV systems, integration of distributed generation, and power conditioning.

Pedro Rodriguez (SM'10–F'13) received M.Sc. and Ph.D. degrees in electrical engineering from the Technical University of Catalonia (UPC), Barcelona, Spain, in 1994 and 2004, respectively. He was a Post-Doctoral Researcher at the Center for Power Electronics Systems, Virginia Tech, USA, in 2005, and at the Department of Energy Technology, Aalborg University (AAU), Denmark, in 2006. He joined the faculty of UPC as an Assistant Professor in 1990, where he became the Director of the Research Center on Renewable Electrical Energy Systems, Department of Electrical Engineering. He is currently a part time Professor with UPC. He was also a Visiting Professor at AAU from 2007 to 2011, and a Co-Supervisor of the Vestas Power Program. In 2011, he joined Abengoa, Seville, Spain, where he was the Director of Technology on Power Systems and Power Electronics. He has been with the Department of Engineering, Loyola University Andalusia as a Professor since 2014. He has coauthored one book, over 70 papers in technical journals and around 250 papers in conference proceedings. He is the holder of twelve licensed patents. He received the Best Technical Letter Award 2012 and the Second Best Paper Award 2012 in the IEEE Transactions on Power Electronics and the Second Best Paper Award 2014 in the IEEE Journal of Emerging and Selected Topics in Power Electronics. His current research interests include distributed power systems, flexible transmission systems, and power conversion.

Dr. Rodriguez is an IEEE Fellow for his contributions in the control of distributed generation, an Associate Editor of the IEEE Transactions on Power Electronics. He was the Vice Chair of the Sustainability and Renewable Energy Committee of the IEEE Industry Application Society.